PNPI/EXL Internal Note 2009 − 01

Geometry of the EXL silicon recoil detector

A. Zalite[1] and Yu. Zalite[2]

Abstract

Description of the first draft version of the EXL silicon recoil detector geometry is presented. This version of geometry is used for the current simulations in the Geant4 framework. Detailed investigations are carried out to define the final detector geometry.

Gatchina, 2009

[1]zalitea@mail.cern.ch
[2]zalite@pnpi.spb.ru

The EXL experiment is proposed to study the structure of exotic nuclei in light-ion induced reactions at the NESR storage ring. The EXL experimental setup comprises a silicon recoil detector for charged particles surrounded by a scintillator hodoscope to detect the punch-through particles and the gamma rays, slow-neutron detectors, forward detectors for fast ejectiles, and an in-ring heavy ion spectrometer [1].

In the given Note a description of the first draft version of the EXL silicon recoil detector geometry is presented. This version of geometry is based (with minor corrections) on the drawings provided by Jan Patrick Meier and is used for the current simulations.

The EXL silicon recoil detector – EXL Silicon Particle Array (ESPA) – consists of double-sided silicon strip detectors (DSSD) and thick lithium drifted silicon detectors Si(Li). In the forward hemisphere the ESPA is divided into four angular regions – D, C, B, A. These regions essentially differ in their geometry in order to meet requirements of various reactions of interest. Two additional angular regions – E′ and E – are foreseen for the backward hemisphere. These regions will be added later (phase II of experiments) and are not included in the current simulations.

As the silicon recoil detector surrounds the gas-jet target, the regions C, B and A are divided into two subregions (Figure 1).

The double-sided silicon strip detectors are designed to measure coordinates of charged particles tracks, energy deposit and time-of-flight for mass identification. The regions D and C (tracking sections for measurement of vertex z coordinate) contain two layers of such detectors – a layer of thin DSSD (thickness of 0.1 mm) and a layer of DSSD (thickness of 0.3 mm), whereas the regions B and A contain only one layer of DSSD (thickness of 0.3 mm). The lithium drifted silicon detectors Si(Li) (thickness of 9 mm) are designed for energy measurement. A possible reduction of thickness of Si(Li) detectors to 6 mm is under consideration.

The region D ($10.0^\circ < \theta < 42.8^\circ$) consists of three rings. Each ring contains three layers of silicon detectors – a layer of thin DSSD, a layer of DSSD and a layer of Si(Li) detectors. The width (azimuthal direction) and the height (polar direction) of the thin DSSD and DSSD are of 90 mm. The width and the height of the Si(Li) detectors are of 95 mm. Corresponding numbers of silicon detectors for each layer are 12 for the first ring, 20 for the second ring and 24 for the third ring. As a whole, the region D contains 56 thin DSSD, 56 DSSD and 56 Si(Li) detectors (Figure 2).

The region C ($41.6^\circ < \theta < 75.7^\circ$) comprises two subregions: $41.0^\circ < \phi < 139.0^\circ$ and $221.0^\circ < \phi < 319.0^\circ$. Each subregion consists of four rings, and each ring contains two layers of silicon detectors – a layer of thin DSSD and a layer of DSSD. The width and the height of all silicon detectors in the region C are of 90 mm. Each layer in the subregion ring contains 11 silicon detectors. As a whole, the region C contains 88 thin DSSD and 88 DSSD (Figure 3).

The region B ($74.7^\circ < \theta < 82.2^\circ$) comprises two subregions: $42.6^\circ < \phi < 137.4^\circ$ and $222.6^\circ < \phi < 317.4^\circ$. Each subregion consists of one ring, which contains four layers of silicon detectors – a layer of DSSD and three layers of Si(Li) detectors. The width of the DSSD is of 90 mm and the height is of 55 mm. The width of the Si(Li) detectors is of 95 mm and the height is of 60 mm. For each subregion, the first two layers contain 9 silicon detectors, whereas the third and the fourth layers contain 11 silicon detectors. As a whole, the region B contains 18 DSSD and 62 Si(Li) detectors (Figure 4).

The region A ($80.0^\circ < \theta < 88.8^\circ$) comprises two subregions: $46.0^\circ < \phi < 134.0^\circ$ and $226.0^\circ < \phi < 314.0^\circ$. Each subregion consists of one ring, which contains two layers of silicon detectors – a layer of DSSD and a layer of Si(Li) detectors. The width and the height of the DSSD and Si(Li) detectors are of 90 mm. Each layer in the subregion ring contains 11 silicon detectors. As a whole, the region A contains 22 DSSD and 22 Si(Li) detectors (Figure 5).

Positions of silicon detectors in the $r - \theta$ plane (middle detectors in case of subregions C, B and A) are shown in Figure 6. It can be seen that in the given lay-out there are small gaps between the last layer silicons in the region D. Similar small gaps are on the boundaries between the regions D and C, as well as C and B. To eliminate these gaps, it is necessary to increase slightly the angular overlap between the corresponding rings.

All the above-mentioned concerning the geometry of the ESPA regions are summarized in Tables 1 − 8. Tables 9 − 16 contain some additional geometry parameters. Estimates of the number of readout channels for different values of pich are presented in Tables 17 − 18.

Tables 1, 2, 15, 16, as well as Figures 7 − 9 were obtained by simulations using the Geant4 package for tracking. Geantino (an auxiliary particle without interactions) was used as a primary particle. All simulations were performed without the vertex spread. Angular coverages of regions (Table 16) were calculated building geometry only for the given region.

Angular coverage of the ESPA in the plane $\theta - \phi$ is shown in Figure 7. Corresponding distributions of events in theta and phi are shown in Figures 8 and 9.

The current ESPA geometry lay-out includes silicon detectors without inactive materials (support structures, readout electronics and so on). Only the vacuum window (a thin foil between the silicon detectors and the scintillator hodoscope), which affects the energy measurement, is taken into account. The losses of the active area close to the edges of the silicon detectors are not explicitly included in the simulation program geometry description.

A distinctive feature of the given ESPA geometry lay-out − an overlap of silicon detectors, i.e. crossing of additional detectors by primary particle. The overlap of silicon detectors takes place between the neighbouring detectors in the layers of the given ring, between the detectors in the neighbouring rings and even between the detectors in the neighbouring regions (see Figures 1 − 6). The overlap of silicon detectors essentially affects the structure of hits leading to a great variety of event types to analyse.

References

[1] EXL Techical Proposal. http://www-linux.gsi.de/∼wwwnusta/tech_report/05-exl.pdf

Region	θ_{min}	θ_{max}
D	10.00	42.82
C	41.61	75.65
B	74.72	82.17
A	80.00	88.80

Table 1: Angular ranges of the ESPA regions in theta, degrees.

Region	Subregion 1		Subregion 2	
	ϕ_{min}	ϕ_{max}	ϕ_{min}	ϕ_{max}
D	0	360	—	—
C	40.96	139.04	220.96	319.04
B	42.62	137.38	222.62	317.38
A	46.02	133.98	226.02	313.98

Table 2: Angular ranges of the ESPA regions in phi, degrees.

Region	Subregions	Rings	Layers
D	1	3	3
C	2	4	2
B	2	1	4
A	2	1	2

Table 3: Number of subregions, rings and layers.

Region	Thin DSSD layers	DSSD layers	Si(Li) layers
D	1	1	1
C	1	1	0
B	0	1	3
A	0	1	1

Table 4: Number of thin DSSD, DSSD and Si(Li) layers.

Region	Thin DSSD		DSSD		Si(Li)	
	Width	Height	Width	Height	Width	Height
D	90	90	90	90	95	95
C	90	90	90	90	—	—
B	—	—	90	55	95	60
A	—	—	90	90	90	90

Table 5: Width and height of the silicon detectors, mm.

Detector	Thickness
Thin DSSD	0.1
DSSD	0.3
Si(Li)	9.0

Table 6: Thickness of the silicon detectors, mm.

Region	Ring	Layer	Detectors
D	1	1, 2 and 3	12
D	2	1, 2 and 3	20
D	3	1, 2 and 3	24
C	1, 2, 3 and 4	1 and 2	11
B	1	1 and 2	9
B	1	3 and 4	11
A	1	1 and 2	11

Table 7: Number of silicon detectors in a layer (region D) or a subregion layer (regions C, B and A).

Region	Thin DSSD	DSSD	Si(Li)
D	56	56	56
C	88	88	—
B	—	18	62
A	—	22	22
Total	144	184	140

Table 8: Number of thin DSSD, DSSD and Si(Li) detectors.

Region	Ring	d_1	d_2	θ
D	1	450.0	460.0	15.71
D	2	470.0	480.0	26.26
D	3	450.0	460.0	36.81
C	1	492.0	497.5	46.84
C	2	480.0	485.5	54.64
C	3	492.0	497.5	62.44
C	4	480.0	485.5	70.24
B	1	450.0	493.0	78.43
A	1	585.0	615.0	84.40

Table 9: Positions of silicon detectors: d_1 – radial positions of detectors in the first layers at $\phi = 90°$ and $\phi = 270°$ (middle detectors in case of subregions C, B and A), $d_2 = d_1 +$ (displacement between detectors in layer), mm; θ – angular positions of rings, degrees.

Region	Ring	Layer	$\Delta\phi$
D	1	1, 2 and 3	30.00
D	2	1, 2 and 3	18.00
D	3	1, 2 and 3	15.00
C	1, 2, 3 and 4	1 and 2	8.27
B	1	1 and 2	10.29
B	1	3 and 4	8.43
A	1	1 and 2	7.95

Table 10: Azimuthal distance $\Delta\phi$ between silicon detectors, degrees.

Distance between layers 1 and 2	100
Distance between layers 2 and 3	20
Displacement between detectors in layer 1	10
Displacement between detectors in layer 2	10
Displacement between detectors in layer 3	15
Displacement between rings	20

Table 11: Parameters of region D, mm.

Distance between layers 1 and 2	100.0
Displacement between detectors in layer	5.5
Displacement between rings	12.0

Table 12: Parameters of region C, mm.

Distance to middle detector: layer 1	450
Distance to middle detector: layer 2	468
Distance to middle detector: layer 3	525
Distance to middle detector: layer 4	560
Displacement between detectors in layers 1 and 2	43
Displacement between detectors in layers 3 and 4	15

Table 13: Parameters of region B, mm.

Distance to middle detector: layer 1	585
Distance to middle detector: layer 2	599
Displacement between detectors in layer	30

Table 14: Parameters of region A, mm.

Region	R_{min}	R_{max}
D	449.9	613.2
C	479.9	601.0
B	449.8	582.2
A	584.8	636.7
ESPA	449.8	636.7

Table 15: Radial dimensions of the ESPA regions, mm.

Region	% of 2π
D	24.76
C	26.32
B	6.43
A	7.27
ESPA	61.99
Overlap of regions	2.79

Table 16: Angular coverage.

Pitch	D	C	B	A	Total
0.1	97,440	153,120	9,360	19,140	279,060
0.2	48,720	76,560	4,680	9,570	139,530
0.3	32,480	51,040	3,114	6,380	93,014
0.4	24,304	38,192	2,340	4,774	69,610
0.5	19,488	30,624	1,872	3,828	55,812
0.7	13,888	21,824	1,332	2,728	39,772
1.0	9,744	15,312	936	1,914	27,906

Table 17: Estimate of number of readout channels in theta for different values of pitch. Height of silicon detectors is reduced by 3 mm.

Pitch	D	C	B	A	Total
0.1	97,440	153,120	15,660	19,140	285,360
0.2	48,720	76,560	7,830	9,570	142,680
0.3	32,480	51,040	5,220	6,380	95,120
0.4	24,304	38,192	3,906	4,774	71,176
0.5	19,488	30,624	3,132	3,828	57,072
0.7	13,888	21,824	2,232	2,728	40,672
1.0	9,744	15,312	1,566	1,914	28,536
1.5	6,496	10,208	1,044	1,276	19,024
2.0	4,816	7,568	774	946	14,104

Table 18: Estimate of number of readout channels in phi for different values of pitch. Width of silicon detectors is reduced by 3 mm.

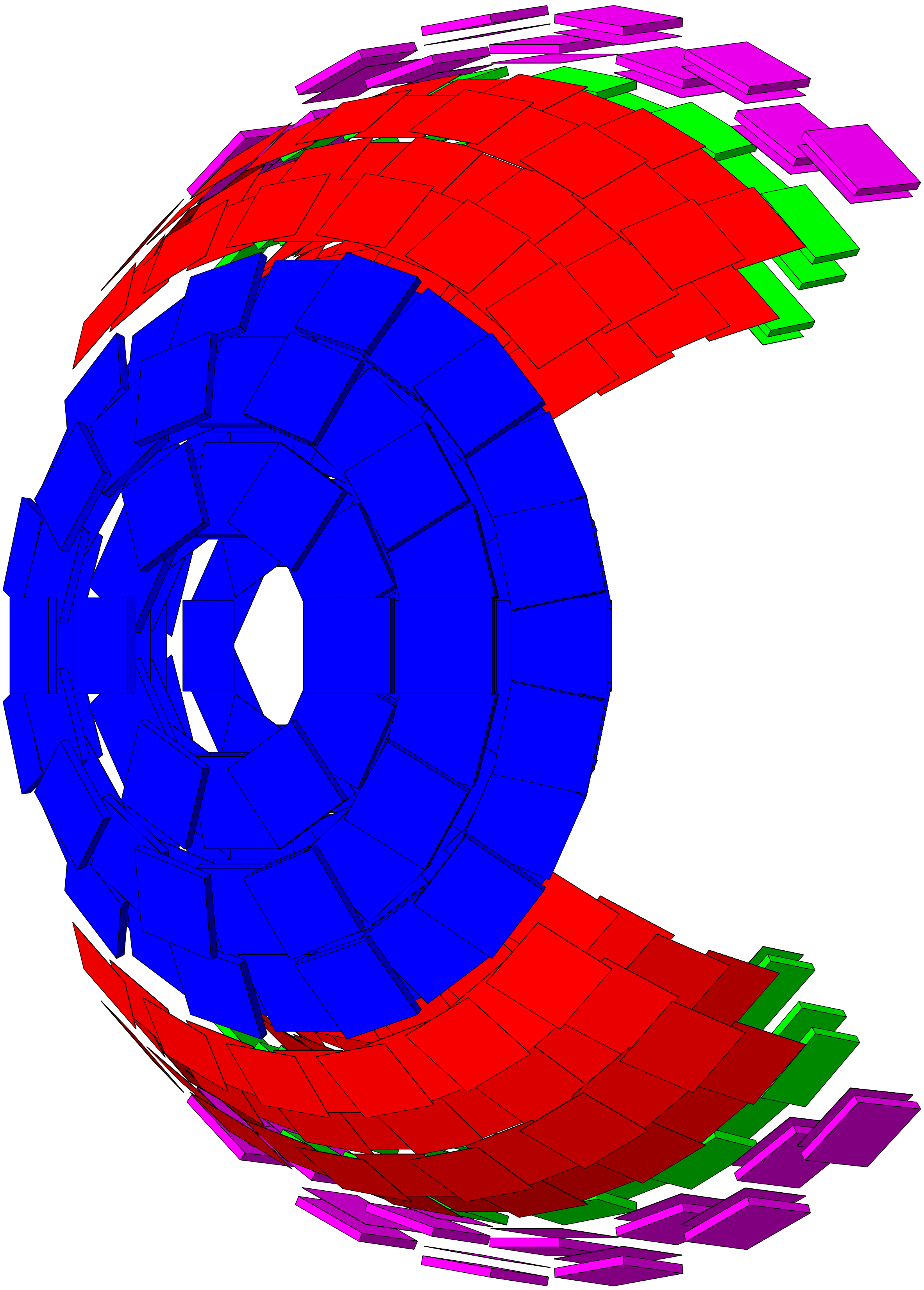

Figure 1: 3D view of the ESPA regions D (blue), C (red), B (green) and A (magenta). Rotation by 90° about z axis is applied.

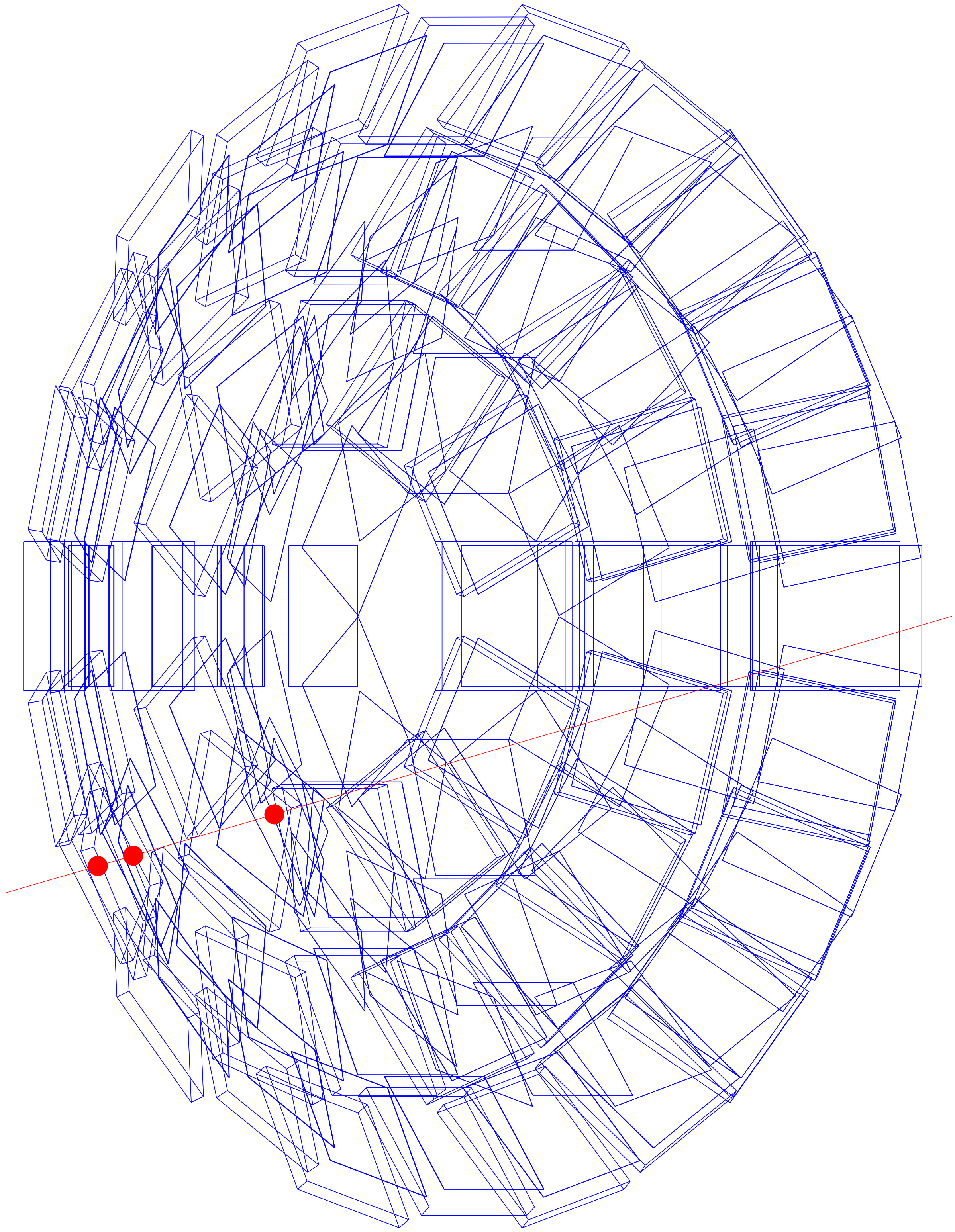

Figure 2: 3D view of the ESPA region D. A random primary particle trajectory and 3 hits are shown.

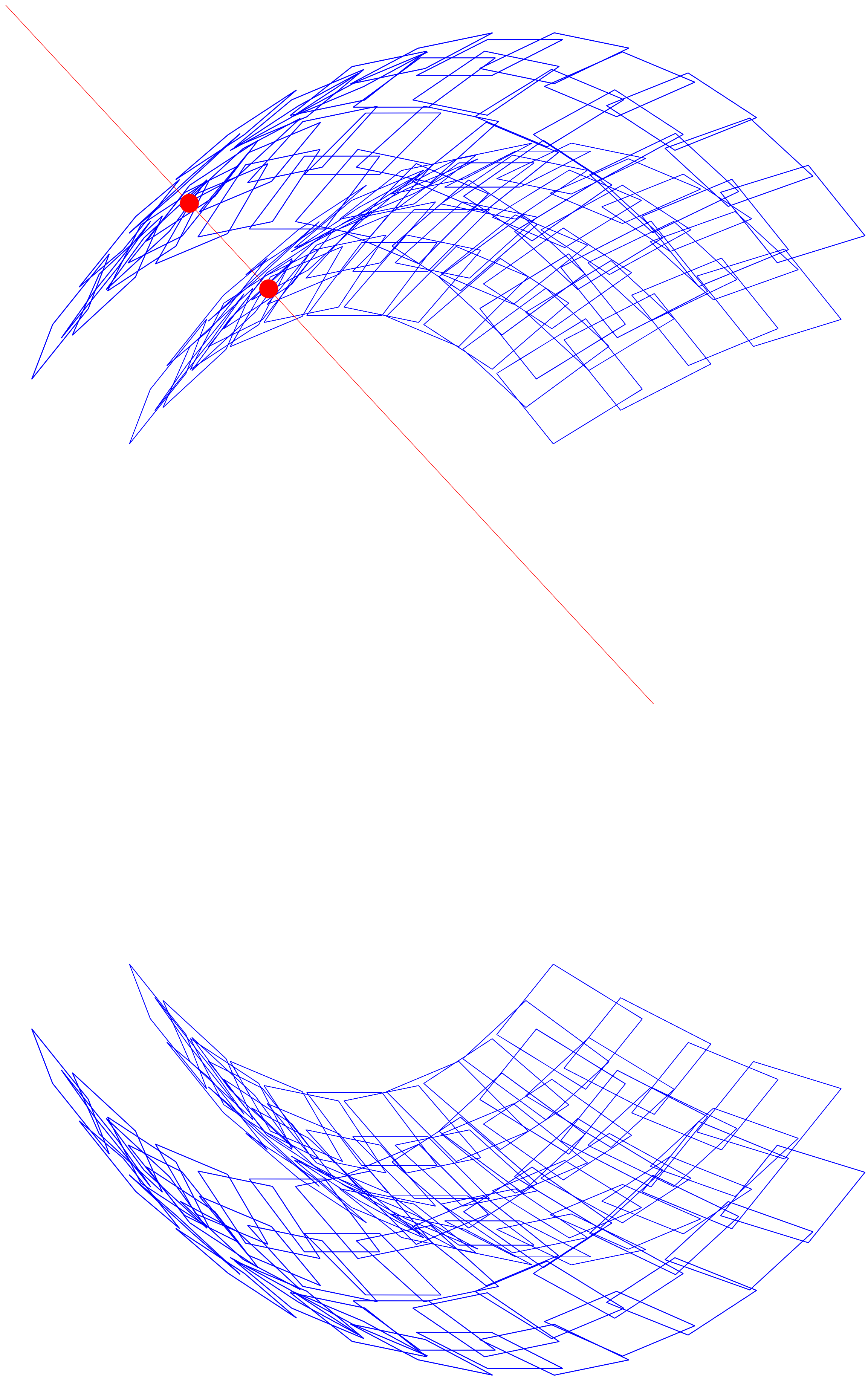

Figure 3: 3D view of the ESPA region C. A random primary particle trajectory and 2 hits are shown. Rotation by 90° about z axis is applied.

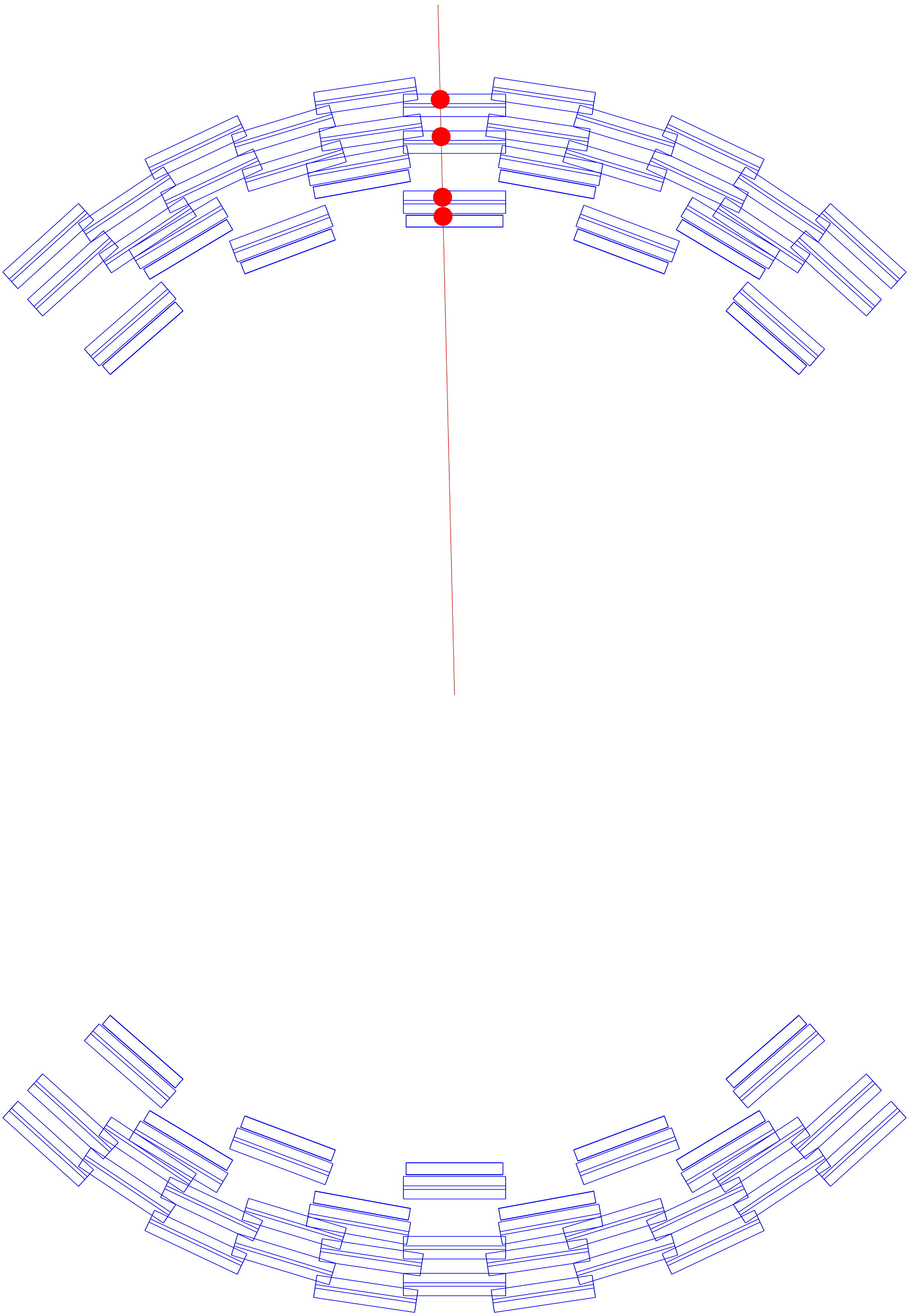

Figure 4: 3D view (along z axis) of the ESPA region B. A random primary particle trajectory and 4 hits are shown. Rotation by 90° about z axis is applied.

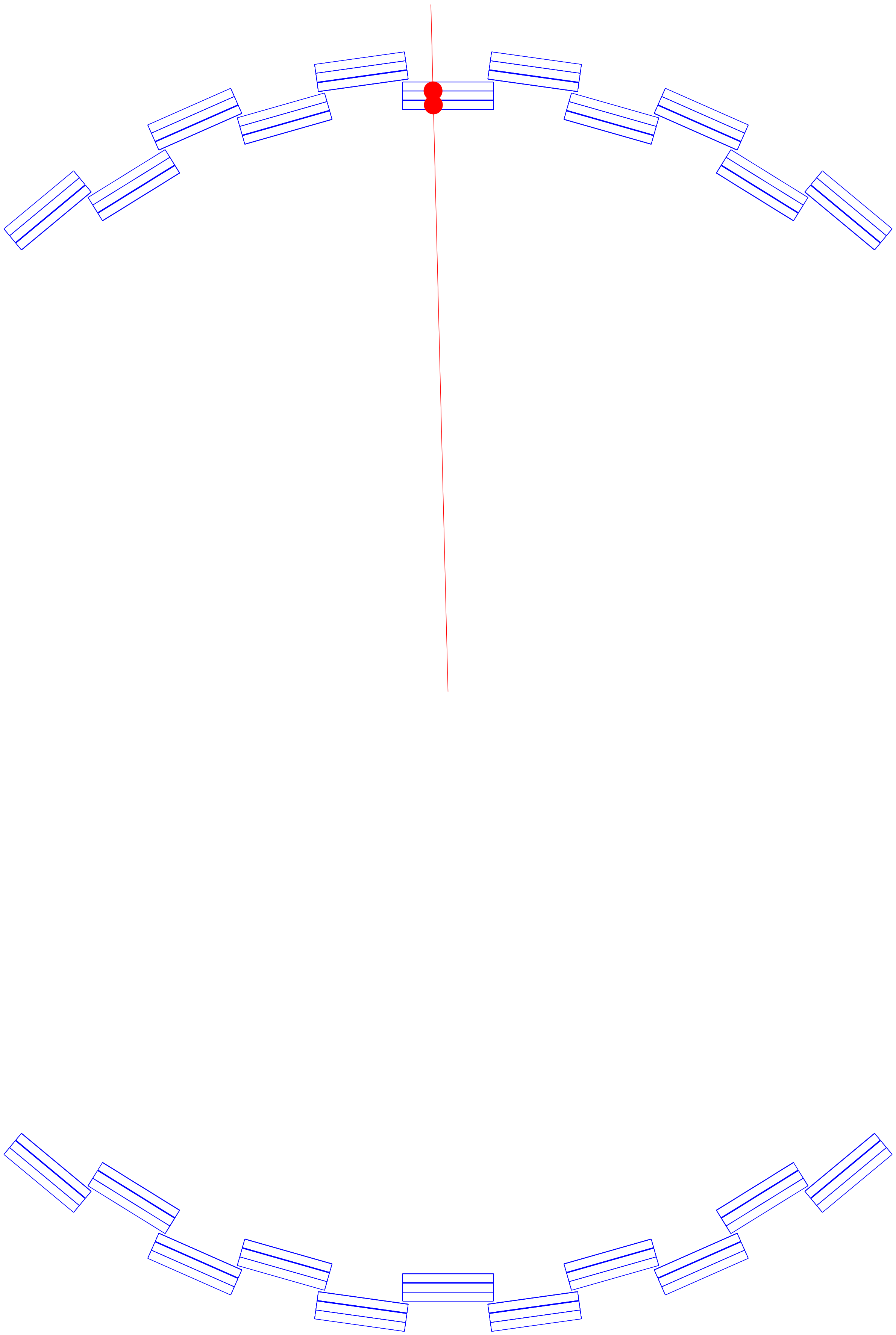

Figure 5: 3D view (along z axis) of the ESPA region A. A random primary particle trajectory and 2 hits are shown. Rotation by 90° about z axis is applied.

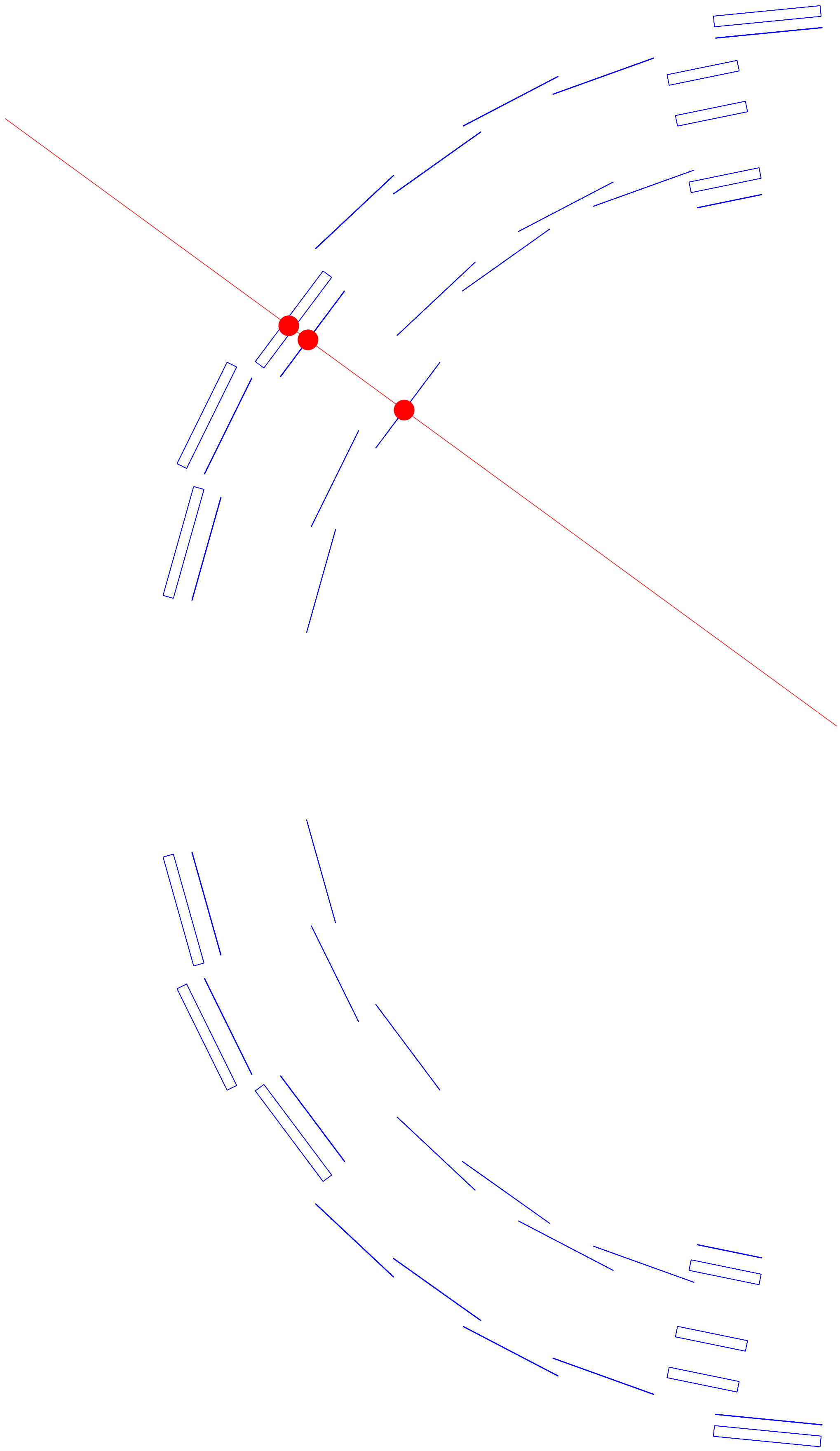

Figure 6: Cross section of the ESPA silicon detectors in the horizontal plane. A random primary particle trajectory and 3 hits are shown.

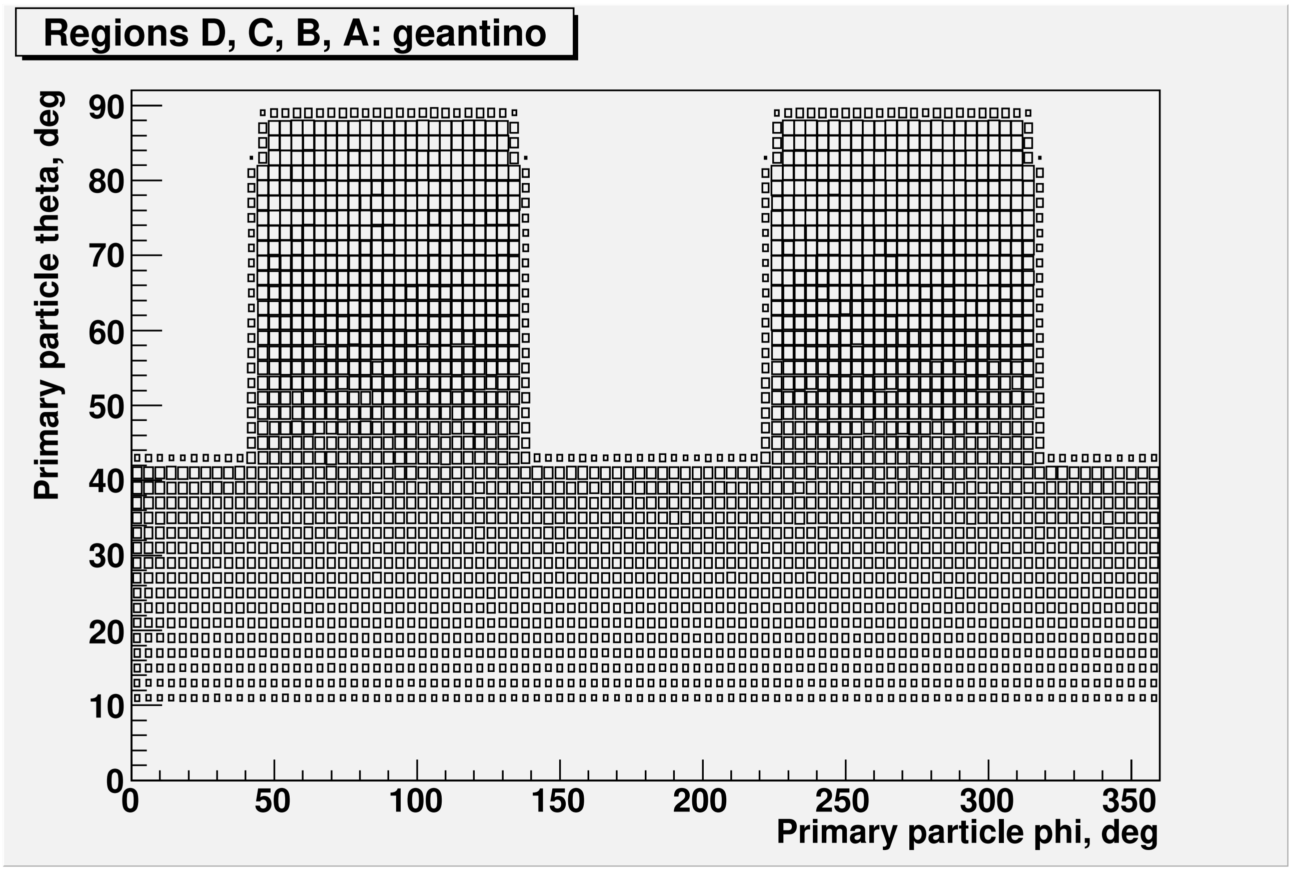

Figure 7: Angular coverage of the ESPA in the plane $\theta - \phi$. Uniform distribution of primary particles over solid angle of 2π has been used.

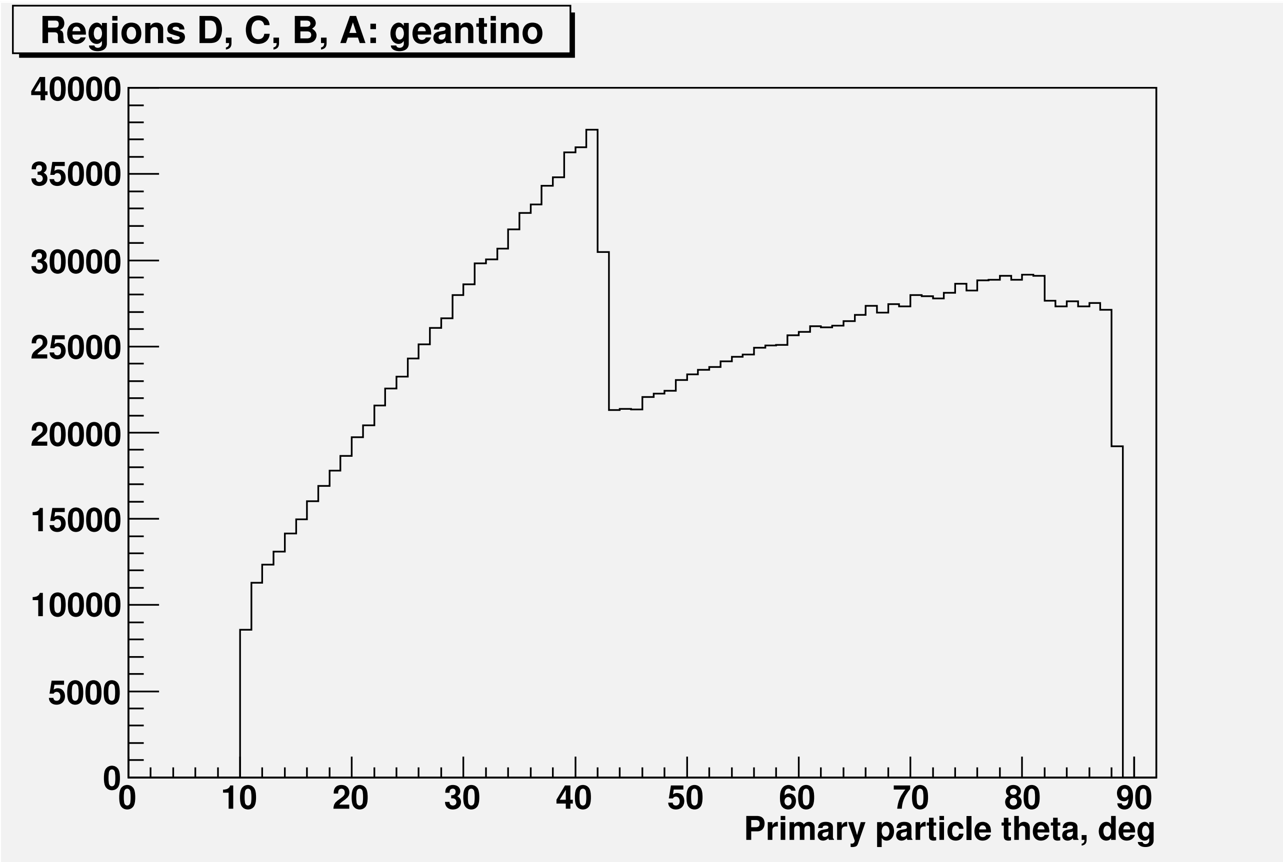

Figure 8: Number of events as a function of theta. Uniform distribution of primary particles over solid angle of 2π has been used.

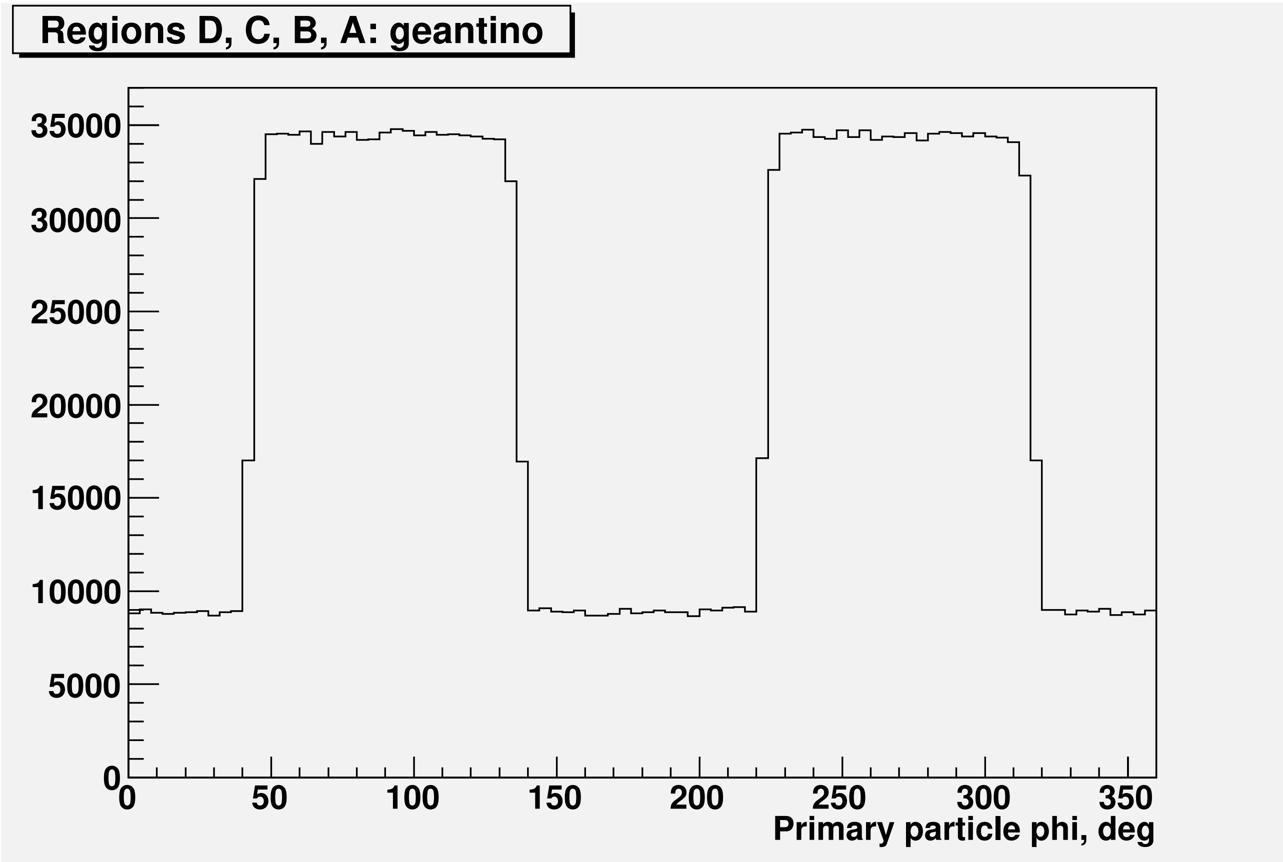

Figure 9: Number of events as a function of phi. Uniform distribution of primary particles over solid angle of 2π has been used.